The Standard Deviation in Fluorescence Correlation Spectroscopy

Thorsten Wohland,* Rudolf Rigler,† and Horst Vogel*
*Department of Chemistry, LCPPM, Swiss Federal Institute of Technology, CH-1015 Lausanne, Switzerland and †Institute of Medical Biophysics, Karolinska Institute, Doktorsringen 6C 3H, 10401 Stockholm, Sweden

ABSTRACT The standard deviation (SD) in fluorescence correlation spectroscopy (FCS) has been mostly neglected in applications. However, the knowledge of the correct SD is necessary for an accurate data evaluation, especially when fitting theoretical models to experimental data. In this work, an algorithm is presented that considers the essential features of FCS. It allows prediction of the performance of FCS measurements in various cases, which is important for finding optimal experimental conditions. The program calculates the SD of the experimental autocorrelation function online. This procedure leads to improved parameter estimation, compared to currently used theoretical approximations for the SD. Three methods for the calculation of the SD are presented and compared to earlier analytical solutions (D. E. Koppel. 1974. *Phys. Rev. A.* 10:1938–1945.), calculation directly from fluorescence intensity values, by averaging several FCS measurements, or by dividing one measurement into a set of shorter data packages. Although the averaging over several measurements yields accurate estimates for the SD, the other two methods are considerably less time consuming, can be run online, and yield comparable results.

INTRODUCTION

Fluorescence correlation spectroscopy (FCS) is a versatile technique for in vivo and in vitro investigations of biomolecular interactions. Described for the first time almost three decades ago by Magde et al. (1972) it has recently found increasing interest as a tool to screen for ligand receptor interactions both in fundamental research (Rauer et al., 1996; Klingler and Friedrich, 1997; Van Craenenbroeck and Engelborghs, 1999; Wohland et al., 1999) and in drug development (Rogers, 1997; Sterrer and Henco, 1997; Auer et al., 1998; Winkler et al., 1999). FCS is based on the statistical analysis of fluctuations in the fluorescence intensity detected from a confocal volume. These fluctuations can be analyzed in terms of autocorrelation functions (ACFs) whose theoretical shape can be predicted from the nature of the underlying molecular process (e.g., translational and rotational diffusion, chemical reactions). The most important step in FCS is the fitting of the parameters of these theoretical models to the experimental data. However, the fitting procedure (usually a nonlinear least-squares fit) depends strongly on the weighting of the data points, i.e., on the knowledge of the standard deviation (SD) of every point in the experimental ACF. It was noted elsewhere that the existing methods to calculate the SD of an FCS measurement usually overestimate the errors and lead to χ^2_v values well below 1 (Rigler et al., 1993; Meseth et al., 1999), although they should converge to 1 for an appropriate fit (Bevington and Robinson, 1992).

In previous studies, the statistical accuracy of FCS measurements has been treated theoretically and experimentally by several authors (Koppel, 1974; Qian, 1990; Kask et al., 1997; Meseth et al., 1999). In these earlier works, the SD of the ACF for diffusion of particles in a probe volume illuminated by a Gaussian laser beam was neither directly calculated nor measured. The diffusion of particles across a focal volume that can be described by a Gaussian profile along all three Cartesian axes gives rise to an ACF that has the form of a hyperbola, but analytical calculations of the variance were done only for exponential functions. Calculations for hyperbolic ACFs were not treated because the integrals involved cannot be solved analytically (Koppel, 1974). Measurements are difficult because the autocorrelators used in FCS are usually hardware correlators and only give access to the experimental autocorrelation function, but not to the intensity signal from which this function is calculated. This intensity signal is necessary for the calculation of the SD. Only recently have correlators become available that can also record the intensity traces (see *www.correlator.com*; Eid et al., 2000). However, no attempts have yet been made to calculate SDs of the ACFs from these traces.

In this article, we present simulations of FCS measurements that allow a detailed theoretical treatment of the SD for the ACF over delay times ranging from 0.2 μs to 50 ms. These simulations are compared with the formula derived by Koppel (1974) for exponential functions. At the same time, we experimentally determined ACFs and calculated their SDs by directly measuring the intensity signals arising from a confocal volume. These measurements corroborate the results of the simulations: (1) Koppel's SD, which was calculated for an exponentially decaying function, can only approximate the real SD; (2) there exist crucial situations in FCS where the weighting of data points with the directly calculated SD yield better parameter estimations than weighting with Koppel's SD.

Received for publication 22 June 2000 and in final form 21 March 2001.
Address reprint requests to Horst Vogel, Swiss Federal Institute of Technology, Department of Chemistry/LCPPM, CH-1015 Lausanne, Switzerland. Tel.: +41-21-693-3155; Fax: +41-21-693-6190; E-mail: horst.vogel@epfl.ch.

0006-3495/01/06/2987/13 $2.00

THEORY

In a FCS experiment, the time course of fluctuations of the fluorescence signal F(t) around the average fluorescence signal $\langle F\rangle$ is measured yielding information on molecular processes or molecular motions. The fluctuations of the fluorescence signal stem from changes either in the number of fluorescent particles or in the fluorescence yield (number of photons per particle and per second) of the particles in the open probe volume, which is defined by the focal volume of a tightly focused laser beam. To analyze these fluctuations, the ACF of the fluorescence intensity is calculated by

$$G(\tau) = \frac{\langle F(0)F(\tau)\rangle}{\langle F(\tau)\rangle^2}. \tag{1}$$

The angular brackets $\langle\ \rangle$ indicate a time average, F is the fluorescence signal as a function of time, and τ is the delay time.

In most FCS experiments, the fluorophores are excited by a laser beam with a Gaussian beam profile, and the emitted fluorescence is observed through a pinhole. Under these conditions, the probe volume can be approximated by a Gaussian distribution in all three Cartesian coordinate axes, further referred to as a GGG profile (Aragon and Pecora, 1976; Rigler et al., 1993). The actual probe volume is defined by a Gaussian laser beam (GLB) profile that is Gaussian in the x- and y-direction and Lorentzian in the z-direction (Eq. 9 and Saleh and Teich, 1991), and by a pinhole that spatially filters the detected intensity. w_0 is defined as the distance from the optical axis and z_0 as the distance along the optical axis, both at which the laser intensity has dropped by $1/e^2$ (including the filtering effect of the pinhole). The parameter $K = z_0/w_0$ describes the shape of the probe volume, which is determined by the size of the laser focus and the pinhole. K should not change if the size of the focus and the pinhole are kept constant.

If only one particle species is observed that undergoes translational diffusion, the ACF is given by (Aragon and Pecora, 1976; Thompson, 1991; Rigler et al., 1993)

$$G(\tau) = \frac{\gamma}{N}\left(1 + \frac{\tau}{\tau_D}\right)^{-1}\left(1 + \frac{\tau}{K^2\tau_D}\right)^{-1/2} + G_\infty. \tag{2}$$

The correlation time τ_D (sometimes referred to as diffusion time) is defined as

$$\tau_D = \frac{w_0^2}{4D}. \tag{3}$$

D is the diffusion coefficient, N is the average number of light-emitting particles diffusing in the focal sample volume. G_∞ is the limiting value of $G(\tau)$ for $\tau \to \infty$, which is generally, 1. γ is a correction factor considering the intensity profile in the focus and is defined according to Thompson (1991) as

$$\gamma = \frac{W_2}{W_1} \tag{4}$$

and

$$W_n = \int\left[\frac{I(r, z)\cdot CEF(r, z)}{I(0, 0)\cdot CEF(0, 0)}\right]^n d\Omega. \tag{5}$$

$I(r, z)$ is the intensity distribution in the focus and $CEF(r, z)$ is the collection efficiency function describing the efficiency of fluorescence detection at different locations in the sample, and $d\Omega$ indicates that the integral is evaluated over all three spatial dimensions. It is assumed that the sample extends considerably beyond the observed confocal volume. Otherwise, the shape of the sample volume would have to be included in the integral in Eq. 5. The number of particles present in the confocal volume can be expressed as

$$N = W_1 \cdot C, \tag{6}$$

where C is the particle number concentration. The factor γ is omitted in the following equations because it is a proportionality constant that influences only the parameter N in Eq. 2 and does not alter any conclusions drawn in this work. It should, however, be borne in mind that the number N now represents an apparent number of particles, and, for absolute concentration measurements, the factor γ has to be included. The relation of the actual number of particles in the confocal volume and the apparent number will be briefly discussed in the Results and Discussion sections.

If several different fluorescent species are present, the model of the ACF (Eq. 2) has to be extended. Taking into account different quantum yields for the general case of R components, one obtains (Thompson, 1991)

$$G(\tau) = \frac{\sum_{i=1}^{R}\alpha_i^2\langle N_i\rangle g_{3di}(\tau)}{\left[\sum_{i=1}^{R}\alpha_i\langle N_i\rangle\right]^2} + G_\infty \tag{7}$$

and

$$g_{3di}(\tau) = \left(1 + \frac{\tau}{\tau_{Di}}\right)^{-1}\left(\frac{1 + \tau}{K^2\tau_{Di}}\right)^{-1/2}. \tag{8}$$

$\alpha_i = Q_i/Q_1$, where the fluorescence yield Q_i of a particle is defined as a product of absorbance, fluorescence quantum efficiency, and experimental fluorescence collection efficiency of the ith species, and τ_{Di} is defined according to Eq. 3 with diffusion coefficients D_i. For $R = 1$, Eq. 7 reduces to Eq. 2.

MATERIALS AND METHODS

The simulated system

In the following, we define the conditions for the computer simulations, which were as close as possible to the conditions used in the real experiments described later. To simulate the fluorescence intensity signals arising from a confocal volume, a certain number of particles were included in a

sphere of 3-μm radius (Fig. 1). If not otherwise stated, we used 69 particles corresponding to a concentration of about 1 nM. Inside the sphere, the excitation intensity I(r, z) was calculated by assuming that a laser beam is focused by a microscope objective (magnification: 63×, numerical aperture (NA) = 1.2) yielding a GLB intensity profile (for laser beam intensity profiles see, for instance, Siegman, 1986)

$$\mathrm{I}(r, z) = \frac{2P}{\pi w_0^2(1 + (z\lambda/\pi w_0^2)^2)} \cdot \exp\left[- \frac{2r^2}{w_0^2(1 + (z\lambda/\pi w_0^2)^2)} \right]. \quad (9)$$

r and z are cylindrical coordinates originating at the center of the sphere, P is the power of the laser beam (100 μW), λ is the wavelength of the laser light (514.5 nm), and w_0 is the radial distance where the intensity has dropped by $1/e^2$ (261.5 nm). A 50-μm-diameter pinhole was assumed to spatially filter the fluorescence light from the sample; it ensures that only light close to the focal plane is collected. The 63× objective yielded a projection of the pinhole to the sample space of 793.7-nm diameter. Using these values, the CEF, which describes the spatial filtering effect of the pinhole, was calculated for the whole sample space (for details, see Qian and Elson, 1991 and Rigler et al., 1993).

Each particle was considered to perform a random walk independently from the other particles. The time steps of the simulation were set to Δ_t = 0.2 μs corresponding to the smallest sampling time of the FCS simulations (see next section). The jump distance of a particle during that time step was determined by a random variable with a Gaussian distribution with center value 0 and an SD = σ, depending on the chosen diffusion coefficient D,

$$\sigma = \sqrt{6D\Delta_t}. \quad (10)$$

The direction of the movement was completely random. At the start of the simulations, a random, uniform distribution of the particles was created inside the sphere. When a particle left the sphere after diffusion, a new particle was randomly created on the surface of the sphere, thus keeping the number concentration inside the sphere constant. Note that the number of particles in the detection volume, which is much smaller than the simulated sphere, still fluctuates freely. At each time step the fluorescence intensity of each particle was determined.

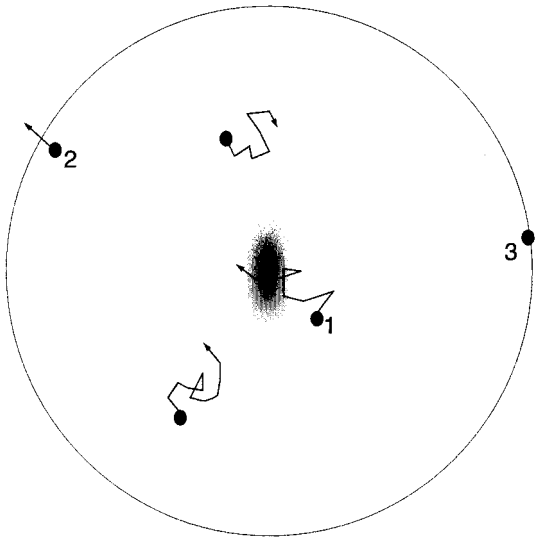

FIGURE 1 The simulated system observed along the optical axis. The circle defines a 3-μm sphere in which diffusion of particles is simulated. The different gray areas in the center show the laser intensity weighted by the collection efficiency function down to the limit where the intensity has dropped to $1/e^2$ of its maximum value. Particles crossing the focus (*particle 1*) contribute to the intensity signal and thus to the ACF. Particles that diffuse out of the simulated sphere (*particle 2*) are replaced by a new particle that is randomly created on the border of the sphere (*particle 3*).

For this purpose we calculated the values of I(r, z) and CEF(r, z) with a finite resolution of 5 nm over the sample space and stored the values in a look-up table. Because of the rotational symmetry of the system around the optical axis, we calculated the values along the radial (r) and axial (z) coordinates over a distance of 3 μm each (600 × 600 values). Thus the resolution for the angle φ is not limited. Compared to the calculation of every value for every particle at each time step, this procedure did not change the results at least to the sixth position after the decimal point but reduced simulation times by 50%.

The fluorescence intensity of the particle depends on the laser intensity at the actual position of the particle, on the absorption cross section (σ_{abs} = 2.2×10^{-20} m^2), and on its fluorescence quantum yield (q_f = 0.98). These chosen values are characteristic for Rho 6G (Hansen et al., 1998; Eggeling et al., 1998). The laser power was set to P = 100 μW, a value typically used in FCS measurements. Around this power level the counts per Rho 6G molecule depend linearly on the excitation intensity (Rigler et al., 1993; Wohland et al., 1999), excluding dye saturation effects. To prove that this holds also for the simulations, the number of photons absorbed per particle have been calculated. The number of photons per area and per second produced by the laser beam is given by I(r, z)/e_{phot}, where e_{phot} is the energy of one photon. The average number of photons n_{abs} absorbed by the molecule with absorption cross section σ_{abs} during a time of Δ_t = 0.2 μs is thus given by

$$n_{abs} = \mathrm{I}(r, z)/e_{phot} \cdot \sigma_{abs} \cdot \Delta_t. \quad (11)$$

Depending on the position of the molecule, the range is $0 \le n_{abs} \le 11$ photons according to Eq. 9. With a lifetime of 3.9 ns (Eggeling et al., 1998), a Rho 6G molecule could theoretically absorb at least 4–5 times more photons in the time of 0.2 μs. We therefore neglect saturation and photobleaching effects in the simulations. Furthermore, we do not take into account possible triplet states of the molecules. In reality, the fluorophore can cross to long-lifetime triplet states, thus reducing the maximum number of fluorescence cycles the molecule can undergo. To calculate the number of emitted photons N_e of a particle, one has to consider the quantum yield q_f of the fluorophore. N_e is therefore given by

$$N_e = n_{abs} \cdot q_f. \quad (12)$$

The number N_d of emitted photons that are detected is determined by the quantum efficiency of the detector q_D, by the CEF, and thus by the position of the particle,

$$N_d = \mathrm{P}(\kappa \cdot N_e \cdot \mathrm{CEF}(r, z) \cdot q_D). \quad (13)$$

P(x) is a random variable following a Poisson distribution with average value x. κ is a constant that describes the detection efficiency of the instrument and intensity losses at mirrors and filters. The random variable ensures that the detected photon counts follow a Poisson distribution as predicted for a stationary light source. However, for freely diffusing particles as assumed in this work, the actual photon count distribution will be broadened due to their random movement (Mandel and Wolf, 1995; Chen et al., 1999). The count rates per particle can be chosen by adjusting the values of I(r, z), σ_{abs}, and κ. With the above-mentioned values and a detection efficiency of ~1%, the photons detected per particle during a second are in the order of 10^5, a typical value for fuorophores like Rho 6G. The ACF for the intensity signal was calculated in parallel as described in the next section.

Calculation of the autocorrelation function

At the center of the simulations is the correlator architecture proposed by Schätzel (1985, 1991) based on multiple sampling and delay times (Fig. 2). This correlator design is used in the ALV 5000 multiple-tau hardware correlator (ALV-Laser, Vertriebsgesellschaft m.b.H., Langen, Germany), which is installed in many FCS instruments, or in the correlators from Correlator.com (Correlator.com, Bridgewater, NJ). These correlators have a quasi-logarithmic time scale where each channel has an individual sampling time (the bin width) and delay time (the delay from the measurement at time 0). With this quasi-logarithmic time-scale structure, which will be described below (for details, see Schätzel, 1991), the sampling time increases with the delay time. This approach offers the advantage that a wide range of delay times can be measured with a limited number of correlation channels. For example, delay times between 0.2 μs and 50 ms can be obtained using only 128 channels. For the same range of delay times, a linear correlator would require 250,000 channels. In the presently used correlator, channels 1–16 have a sampling time of 0.2 μs. Each following group of eight channels has an individual sampling time of twice that of the preceding group (channels 17–24, 0.4 μs; channels 25–32, 0.8 μs; up to channels 121–128, 3.2768 ms). The delay time of each channel is the accumulated sampling time of all preceding channels (channel 1, 0 μs; channel 2, 0.2 μs; . . . channel 17, 3.2 μs; channel 18, 3.6 μs; up to channel 128, 49.152 ms). Additional to each channel there is a delayed monitor M_{del} that accumulates all counts sampled in that channel. For every group of channels with equal sampling time (the first 16 channels and each following group of eight channels), there exists a direct monitor M_{dir} that accumulates all counts without delay time at a particular sampling time.

For the calculation of the ACF, every channel is multiplied according to its delay time by a channel at 0 delay time, that possesses the same sampling time. For example, channels 1–16 (delay times 0–3.0 μs, sampling time 0.2 μs) are multiplied by the intensity signal that is presently measured during 0.2 μs (delay time 0, sampling time 0.2 μs). Channels 17–24 (delay times 3.2–6.0 μs, sampling time 0.4 μs) are multiplied by the intensity signal that is presently measured during 0.4 μs (delay time 0, sampling time 0.4 μs). The results of the multiplication are summed up over time for the calculation of the ACF. The counts of each channel are accumulated in its delayed monitor M_{del}. The counts of the sample at delay time 0 with sampling times of 0.2 μs, 0.4 μs, etc. are summed up in the

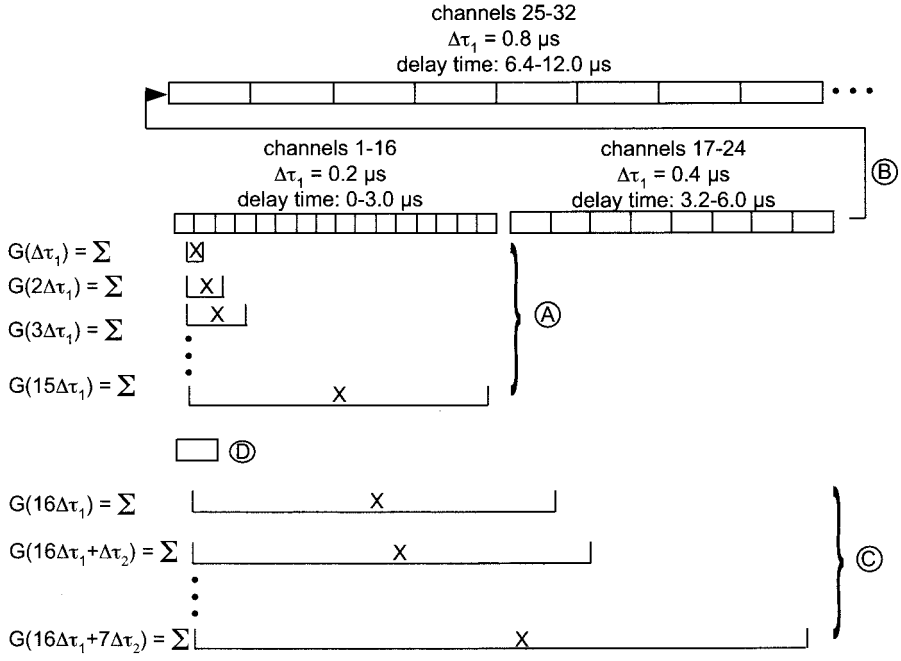

FIGURE 2 Channel architecture of the correlator. (*A*) The fluorescence intensity from the confocal volume is registered with a channel width of 0.2 μs. After every measurement, three tasks are executed: (1) all channels are shifted to the right, channel ($n - 1$) to channel n, channel ($n - 2$) to channel ($n - 1$), . . . , channel 1 to channel 2. The new measurement is stored in channel 1. (2) The products (depicted as X) of channel 1 and 2, of channel 1 and 3, etc., are calculated and added (depicted as Σ) to the correlation function $G(\Delta\tau_1)$, $G(2\Delta\tau_1)$, $G(3\Delta\tau_1)$, etc., respectively. The value of $G(0)$ can be calculated by multiplying channel 1 with itself. (3) The delayed monitor is a register for every channel that sums up all counts that pass through a channel (not shown). Therefore, after each shift of channels the content of every channel is added to its delayed monitor. (*B*) Channels 15 and 16 are summed up and shifted to channel 17 which now acquires a width of 0.4 μs. This happens at the end of every channel group. The last two channels with 0.4-μs width (channel 23 and 24) are added to yield channel 25 with 0.8-μs width and so on. (*C*) Those channels that have a width of larger than 0.2 μs (all channels after channel 16) are now correlated with a channel at 0 delay time of equal length. To achieve this, several channels can be summed up. Channels $1 + 2$ act as the 0-delay-time channel for channels 17–24 (0.4 μs). The sum of channels 1–4 act as 0-delay-time channel for channels 25–32 (0.8 μs), and so on. Note that, for channels 1–16, the correlation is performed after every 0.2-μs measurement, but, for channels with a width of 0.4 μs, the correlation will be done only every 0.4 μs, i.e., after 2 measurements of 0.2 μs and so on. (*D*) The 0-delay-time channel with 0.4-μs width is shown. It is used for the correlations of channels with a width of 0.4 μs. The direct monitor (not shown) is a register for every group of channels with equal length. In this register, the counts are stored that pass through the channel at 0 delay time. Therefore, the 0-delay-time channel will be added to the direct monitors after the correlation for a group of channels with equal width. For example, the 0-delay-time channel of 0.2 μs will be added to the direct monitor for channels 1–16 every 0.2 μs. The 0-delay-time channel of 0.4 μs will be added to the direct monitor for channels 17–24 every 0.4 μs, etc. All correlation functions and monitors are calculated according to Eqs. 14–16.

direct monitor M_{dir} of each group of channels with equal sampling time. The ACF is then calculated by

$$G_i(m\Delta\tau_i) = \frac{\frac{1}{M-m}\sum_{k=1}^{M-m} n(k\Delta\tau_i)n(k\Delta\tau_i + m\Delta\tau_i)}{M_{dir,i}\cdot M_{del,i}}, \quad (14)$$

with

$$M_{del,i} = \frac{1}{M-m}\sum_{k=m}^{M} n(k\Delta\tau_i) \quad (15)$$

and

$$M_{dir,i} = \frac{1}{M-m}\sum_{k=1}^{M-m} n(k\Delta\tau_i). \quad (16)$$

Here, m is an integer, $\Delta\tau_i$ is the sampling time (channel width) of channel i, and $m\Delta\tau_i$ is the delay time. M is the number of measurements over a period of $\Delta\tau_i$, and is given by $M = T/\Delta\tau_i$, where T is the total measurement time. $n(k\Delta\tau_i)$ is the number of photons at time $k\Delta\tau_i$, sampled with a channel width of $\Delta\tau_i$, and $n(k\Delta\tau_i + m\Delta\tau_i)$ the number of photons at time $m\Delta\tau_i$ later. $M - m$ is the number of possible products $n(k\Delta\tau_i)n(k\Delta\tau_i + m\Delta\tau_i)$ over which the summations extend in Eqs. 14–16. The ACF is symmetrically normalized (Schätzel et al., 1988; Schätzel, 1991) with the direct and delayed monitors $M_{dir,i}$ and $M_{del,i}$ of corresponding channel i, respectively.

The standard deviation derived by Koppel

Knowledge of the SD of the ACF is necessary for accurate data analysis (Di Cera, 1992), but its analytical calculation is not possible because it involves diverging integrals for decaying functions of the form given in Eq. 2. To date, the SD has been calculated most often according to an equation derived by Eq. 34 in Koppel (1974). Koppel's equation was derived for the case of exponential ACFs, assuming a high number of particles in the observation volume, negligible background, uniform illumination, and sampling times much smaller than the correlation time expected for the process under investigation. At least the first three conditions are usually not fulfilled in typical FCS experiments. Nevertheless, this formula can be used as an approximation replacing the exponential functions by the correlation function for diffusion (Rigler et al., 1993; Meseth et al., 1999). Because Koppel's formula does not include a normalization factor, we include a factor $\langle n\rangle^{-4}$ to account for the normalization performed by the correlator (see previous section); $\langle n\rangle$ is the average count rate per correlator channel during the measurement. This analysis leads to the following expression for the σ_{Koppel} of the correlation function $G(\tau)$:

$$\sigma^2_{Koppel}(m\Delta\tau_i) = \frac{1}{M}\frac{1}{N^2}\left[\frac{(1+g^2(\Delta\tau_i))(1+g^2(m\Delta\tau_i))}{1-g^2(\Delta\tau_i)} + 2mg^2(m\Delta\tau_i)\right] + \frac{1}{M}\left[\frac{2(1+g^2(m\Delta\tau_i))}{N\langle n\rangle} + \frac{1}{\langle n\rangle^2}\left(1+\frac{g(m\Delta\tau_i)}{N}\right)\right], \quad (17)$$

where the variables have the same meanings as in Eqs. 14–16, and N is the average number of particles in the observation volume. For the function $g(\tau)$, we insert the model for simple three-dimensional diffusion $g_{3di}(\tau)$ as defined in Eq. 8.

The calculation of σ_{Koppel} needs initial estimates of $\langle n\rangle$, N, K, and τ_D before a fit can be performed. For initial estimates $\langle n\rangle$ was calculated from the overall count rate given by the simulation or experiment. For the simulated ACF, N can be estimated from the value of $G(0)$ (shot noise is not considered in the simulations). For the experimental ACF, $G(0)$ has to be approximated by the value of the ACF at small delay times (the channel at 0 delay time cannot be used because of shot noise contributions and is usually not used for fitting). N can then be approximated from this value using Eq. 2 and neglecting the proportionality factor γ. The correlation time τ_D was estimated from the experimental/simulated ACF at the time the ACF has dropped to half its amplitude $G(0)$. An initial value of K can be estimated by prior calculations using the laser intensity profile (Eq. 9). These procedures give only a rough estimate of the parameters, and they are only approximated within a factor 2–3 of the correct values. Because the variations of σ_{Koppel} are small within the error margins of the fit parameters, the method is sufficiently accurate for all purposes within one iteration step.

However, this estimation of the SD is only an approximation of the real SD (Koppel, 1974). This problem can be solved by calculating the SD directly from the intensity signal as proposed in the next section.

Methods to calculate the standard deviation

Contrary to the analytical formula calculated by Koppel (Eq. 17) we determined the SD of the ACF by three different methods using directly the measured intensity traces and ACFs.

In the first method, we determined the SD by calculating the standard error of the mean for each point $G(m\Delta\tau_i)$ of the ACF:

$$\sigma_{IT}(G(m\Delta\tau_i)) = \frac{\left[\frac{1}{M-m}\left(\sum_{k=1}^{M-m} n^2(k\Delta\tau_i)n^2(k\Delta\tau_i + m\Delta\tau_i)\right) - \frac{1}{(M-m)^2}\left(\sum_{k=1}^{M-m} n(k\Delta\tau_i)n(k\Delta\tau_i + m\Delta\tau_i)\right)^2\right]^{1/2}}{\left(\sqrt{M-m}\cdot M_{dir,i}\cdot M_{del,i}\right)}. \quad (18)$$

The use of the standard error of the mean (Davenport and Root, 1958) is justified because each value in the ACF is an average over the whole measurement time, and we are only interested in the deviation of this average value from the real value. Strictly speaking, this is only true for uncorrelated signals, i.e., if the products $n(k\Delta\tau_i)n(k\Delta\tau_i + m\Delta\tau_i)$ are independent for different values of the index i. However, it can be used as a first approximation.

In the second method, we calculated the SD by averaging several simulated/measured normalized ACFs. It should be noted that, according to Koppel (1974), the FCS signal is the correlation level above the accidental correlation background given by G_∞, the convergence value of the ACF for long times, and is thus given by

$$G(m\Delta\tau_i) - G_\infty. \quad (19)$$

The SD therefore must be calculated for these values and not for $G(m\Delta\tau_i)$. Another problem arising is that $G(m\Delta\tau_i) - G_\infty$ does not only depend on the expected error of the ACF but also on the average number of particles in the observation volume. This does not pose a problem for the simulations where the number of particles is constant on average, but, in an experiment, the number of particles can change in time due to absorption processes, stoichiometry of binding, depletion of particles due to photolysis, unspecific adsorption to sample containers, or other phenomena. This change of amplitude does not reflect the uncertainty of the ACF measurement but a systematic error inherent in the sample. If this is not taken into account, the SD will be overestimated due to the change in amplitude caused by changes in the number of particles. We therefore define first a normalized average value for all points of the ACFs,

$$\bar{g}(m\Delta\tau_i) = \frac{1}{L}\sum_{\ell=1}^{L}\frac{G_\ell(m\Delta\tau_i) - G_{\ell,\infty}}{G_\ell(0) - G_{\ell,\infty}}. \quad (20)$$

Here, L is the number of ACFs averaged, and ℓ is their index. The SD is thus calculated by

$$\sigma_{AV}(m\Delta\tau_i) = \sqrt{\frac{1}{L-1}\sum_{\ell=1}^{L}\left(\frac{G_\ell(m\Delta\tau_i) - G_{\ell,\infty}}{G_\ell(0) - G_{\ell,\infty}} - \bar{g}(m\Delta\tau_i)\right)^2}. \quad (21)$$

The values for $G_\ell(0)$ and $G_{\ell,\infty}$ can be estimated by either averaging over the first (short delay times) and last (long delay times) points of the ACF or by using the parameter estimations of a fit without data weighting (the method used in this work). This is possible because the estimated number of particles N in the observation volume depends only weakly on the fit method (see Results and Discussion and Table 1). The value of σ_{AV} is valid for a normalized ACF. For a fit to a non-normalized ACF, it has to be rescaled to the real amplitude of the ACF to be evaluated.

In the third method, we used the same procedure as described before (Eqs. 20 and 21) but applied it to S subsets of one single measurement with measurement time T, i.e., we divided the intensity trace of one single measurement in S subsets of length T/S. The ACF was calculated for each subset and for the whole measurement. σ_{AV} was then calculated for the subsets. σ_{AV} is a valid estimate for the SD of an ACF that was measured for the time T/S. To obtain the SD for the ACF over the entire measurement time T, we divide σ_{AV} by the square root of S:

$$\sigma^*_{AV}(m\Delta\tau_i) = \frac{\sigma_{AV}(m\Delta\tau_i)}{\sqrt{S}}. \quad (22)$$

Eq. 22 is a direct result from the fact that the SD decreases with the square root of the measurement time.

Calculation of the factor γ

The factor $\gamma = W_2/W_1$, as defined in Eqs. 4 and 5, can be calculated by numerical integration with the values of $I(r, z)$ and $CEF(r, z)$ values as stored in the look-up table. The W_n then have the form,

$$W_n = 2\pi \cdot \sum_i \sum_j \left[\frac{I(i\cdot\Delta r, j\cdot\Delta z)\cdot CEF(i\cdot\Delta r, j\cdot\Delta z)}{I(0,0)\cdot CEF(0,0)}\right]^n \cdot i\cdot\Delta r^2\cdot\Delta z. \quad (23)$$

i and j are the summation indices over the sums in the radial (r) and axial (z) direction, respectively. The integration over the radial angle leads to the factor 2π. Δr and Δz are the distances on the grid (5 nm). The extra factor $i\Delta r$ is the Jacobian determinant (Grossmann, 1988; Bronstein and Semendjajew, 1989) resulting from the transformation of Cartesian coordinates to cylindrical coordinates. The summation that replaces the integration in Eq. 5 takes place over the whole sample volume, i.e., the sphere of 3-μm radius. Because the CEF and the intensity distribution converge to 0 at the borders of the sample volume, this is a good approximation to an integration over the whole space up to infinity.

The simulations

The simulation program was written in the programming language C (MIPSpro Compiler, Version 7.2.1) and ran on an O2 Workstation under

TABLE 1 Two-component fits

	τ_1 and τ_2 Free			
	System A		System B	
	τ_1 (μs)	τ_2 (ms)	τ_1 (μs)	τ_2 (μs)
Calculated	63.3	5.1	63.3	253.1
1-comp. simulation	58.8 ± 3.9	4.9 ± 0.9	58.8 ± 3.9	250.0 ± 19.8
No weighting	54.8 ± 6.7	4.2 ± 0.9	72.8 ± 13.2	335.0 ± 104.8
Weighting				
σ_{Koppel}	54.7 ± 6.1	4.2 ± 0.9	65.7 ± 13.7	298.9 ± 91.7
σ_{IT}	55.3 ± 5.5	4.2 ± 0.8	66.0 ± 14.0	295.5 ± 95.7
σ_{AV}	57.9 ± 6.2	4.4 ± 0.9	64.4 ± 13.6	282.4 ± 81.2
	τ_1 Fixed to 58.8 μs, τ_2 Free			
	System A, τ_2 (ms)		System B, τ_2 (μs)	
No weighting	4.5 ± 0.6		241.7 ± 29.1	
Weighting				
σ_{Koppel}	4.5 ± 0.7		254.1 ± 29.0	
σ_{IT}	4.5 ± 0.6		250.5 ± 29.0	
σ_{AV}	4.5 ± 0.7		250.4 ± 30.6	

Correlation times (τ_1, τ_2) obtained by fitting simulated two-component systems (System A, $D_1 = 2.7 \times 10^{-10}$ m^2/s, $D_2 = 3.33 \times 10^{-12}$ m^2/s; System B, $D_1 = 2.7 \times 10^{-10}$ m^2/s, $D_2 = 6.75 \times 10^{-11}$ m^2/s). The correlation times under "Calculated" are the values determined by Eq. 3.

The values noted under "1-Comp. simulation" are the correlation times obtained by simulating and evaluating one-component systems. All other rows represent values from two-component simulations. "No weighting" indicates the results obtained by fitting the simulations with two-component models but without weighting the data points. The other rows give the correlation times when the data points are weighted either with σ_{Koppel}, σ_{IT}, or σ_{AV}. The number of particles N was not influenced by the different fit procedures, and was $N = 0.169 \pm 0.012$ (mole fraction for slower diffusion particles $y = 0.47 \pm 0.08$) and $N = 0.184 \pm 0.003$ ($y = 0.42 \pm 0.13$) for System A and System B, respectively. K was fixed to 2.7 for all simulations.

In the upper part of the table, both diffusion times were free parameters in the fit. In the lower part, τ_1 was fixed to its value obtained by one-component simulations ($\tau_1 = 58.8$ μs).

All values are obtained by averaging 10 simulations.

Irix 6.5 (Silicon Graphics, Schlieren, Switzerland). In all simulations, we used a measurement time of ~6.7 s (2^{25} intervals of 0.2 μs). The random numbers were created by a portable number generator called ran1 (Press et al., 1992) that has a period of about 2×10^9. In our simulation, we calculated 2^{25} steps for 69 particles, and, for every particle, three random numbers for the movement in space, and one random number for the emission and detection processes. Thus $69 \times 4 \times 2^{25} \approx 9.3 \times 10^9$ random numbers were obtained, exceeding the period of the random-number generator by a factor 5. But each of the 69 particles is observed, on average, not longer than ~8 ms ($<4 \times 10^4$ steps), that is the time the particle needs, on average, to traverse the sphere of 3-μm radius (Eq. 3). This particle is then replaced by another one with random coordinates on the border of the sphere. Thus, individual particles are simulated for much smaller times than the period of the random-number generator. Furthermore, correlations should emerge on the time scale of the period exhaustion of the random-number generator, i.e., at delay times of about 1 s. However, the ACFs are not calculated for such long delay times.

Press et al. (1992) proposed another random-number generator (ran2) with a period of about 10^{18}, thus, largely exceeding the number of steps in our calculations. Simulations can be run as well with this generator but they increase the computation time by more than 50% and the fit parameters and χ^2_v values do not change within the margin of error (ran2: $N = 0.177 = 0.003$, $\tau_D = 57.3 \pm 3.2$ μs, $K = 2.8 = 0.5$, $G_\infty = 0.992 \pm 0.005$, χ^2_v (σ_{IT}) $= 0.76 \pm 0.18$; compare with the Results and Discussion section). Computation times are about 1 h for a 1-s simulated measurement using the random-number generator ran1.

First, a series of tests were run on one-component situations to investigate how the simulations depend on the concentration, diffusion coefficient, absorption cross section, and measurement time. Then, two series of two-component simulations were run. All particles were assumed to have the same photophysical characteristics, but about half the particles (34 of 69) had a lower diffusion coefficient. Although the fast component always had a diffusion coefficient of $D_1 = 2.7 \times 10^{-10}$ m^2/s, the value of D_2 was assumed to be 3.33×10^{-12} m^2/s in system A and 6.75×10^{-11} m^2/s in system B. These systems represent the extreme cases where either the diffusion coefficients are sufficiently different to allow a distinction by FCS (a factor 81 in system A) or where the difference is close to the resolution limit of FCS (a factor 4 in system B, (Meseth et al., 1999)). If not otherwise stated, the count rate was ~35 kHz per particle. For every investigated system, at least five simulations were performed and averaged. Typical ACFs for the one- and two-component cases are depicted in Fig. 3.

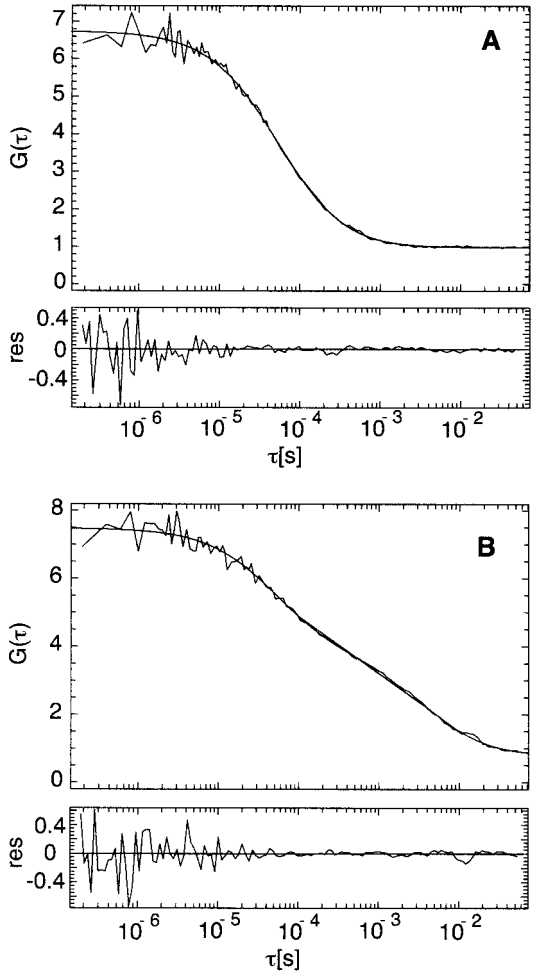

FIGURE 3 (*A*) One-component simulation with fitted function and residuals. $D = 2.7 \times 10^{-10}$ m^2/s, $P = 100$ μW, $\lambda = 514.5$ nm, $\sigma_{abs} = 2.2 \times 10^{-20}$ m^2, $q_f = 0.98$, simulation time is 6.7 s, 69 particles are simulated in a sphere of 3-μm radius (corresponding to a concentration of 1 nM), 50-μm diameter pinhole. (*B*) Two-component simulation with fitted function and residuals. Thirty-four particles with a diffusion coefficient of $D = 2.7 \times 10^{-10}$ m^2/s and 35 particles with $D = 3.3 \times 10^{-12}$ m^2/s. All other parameters as in (*A*).

Data Analysis

The fitting of the ACFs was done with the Levenberg–Marquardt algorithm from Mathematica 3.0 (Wolfram Research Inc., Champaign, IL). As a measure for the goodness of the fit, we used the χ^2_v statistics. This value measures the difference between the fitted function $y(x)$ and the experimental data y_i at points x_i weighted by σ_i as a sum over all data points i,

$$\chi^2 = \sum_i [(y(x_i) - y_i)/\sigma_i]^2. \quad (24)$$

σ_i is the SD of the experimental point i. To compare different fits, the reduced $\chi^2_v = \chi^2/(\nu - p)$ is calculated (ν = number of points used, p = free parameters in the fit). For an introduction to the calculation of χ^2_v and other statistical parameters, see, e.g., Bevington and Robinson (1992).

Fits were run in four different ways:

1. without weighting the data points,
2. by weighting the data points with the analytical SD of Koppel (σ_{Koppel}, Eq. 17),
3. by weighting the data points with the SD directly calculated from the intensity traces (σ_{IT}, Eq. 18), and
4. by weighting the data points with the SD calculated from several (5–10) ACFs (σ_{AV}, Eqs. 20–21).

For cases 2–4, the value of χ^2_v is calculated with the corresponding SD. For case 1, no value of χ^2_v is calculated because no SD is defined.

For the real FCS experiments, the same data evaluation schemes were used; additionally, fits were run by calculating the SD according to Eq. 22 by dividing one measurement in several subsets and calculating the SD by averaging over the ACFs of the subsets (σ^*_{AV}). The data were fitted with a one- or two-component model as appropriate (Fig. 3). For the one-component fits, we used Eq. 2 with N, τ_D, K, and G_∞ as free parameters. For the two-component fits, Eq. 7 was used, assuming $R = 2$ and N_i, τ_{D1}, τ_{D2}, and G_∞ as free parameters; K was fixed to 2.7, a value determined from the one-component fits (see Results and Discussion).

FCS Experiments

Our home-built fluorescence correlation spectrometer, at the Swiss Federal Institute of Technology in Lausanne, was centered around an inverted

Axiovert 100 TV microscope (Carl Zeiss, Oberkochen, Germany). It consists of a Coherent INNOVA Sabre Ar^+-Laser (Coherent, Inc. Santa Clara, CA) with an output beamwaist of 3 mm. The 514-nm line was used for the excitation of the fluorophores. The laser beam was expanded to 6 mm by a Keplerian beam expansion and was then directly reflected by a dichroic mirror (FT540, Omega, Brattleboro, VT) into the microscope objective (63× C-Apochromat, NA 1.2, water immersion with coverslip correction for a thickness between 0.16 and 0.18 μm, Carl Zeiss). The beam expansion ensured that the back aperture of the microscope objective was fully illuminated to provide a tightly focused laser beam. The fluorescence signal of the sample was collected with the same objective and passed a band pass filter (565DF72, Omega) to reduce the background signal. A 50-μm diameter pinhole was installed in an image plane of the microscope to discriminate against out-of-focus signals. The collected fluorescence light was then focused onto an avalanche photo diode (SPCM-AQ-161, EG&G, Vaudreuil, Canada). The electrical signal was fed into a data acquisition board (PCI-MIO-16E-1, National Instruments, Geneva, Switzerland), that was programmed to count the arriving photons in time intervals of 5 μs and stored up to 10^6 of such measured channels.

The power of the laser beam entering the microscope was set to 100 μW for all experiments. This power level creates reasonably high fluorescence signals per Rho 6G molecule, but was still low enough to keep photobleaching and triplet-state population negligible. The actual power in the confocal volume was not measured but is lower than 100 μW due to losses at lenses, beam splitter, and dichroic mirror.

The sample was deposited in the form of 100-μl droplets on a coverslip with a thickness between of 0.15 and 0.17 mm. From FCS measurements of an aqueous solution of Rho 6G (Molecular Probes, Eugene, OR) the ACF and SD were calculated by the simulation program using the experimental instead of the simulated intensities. Ten measurements were conducted in total.

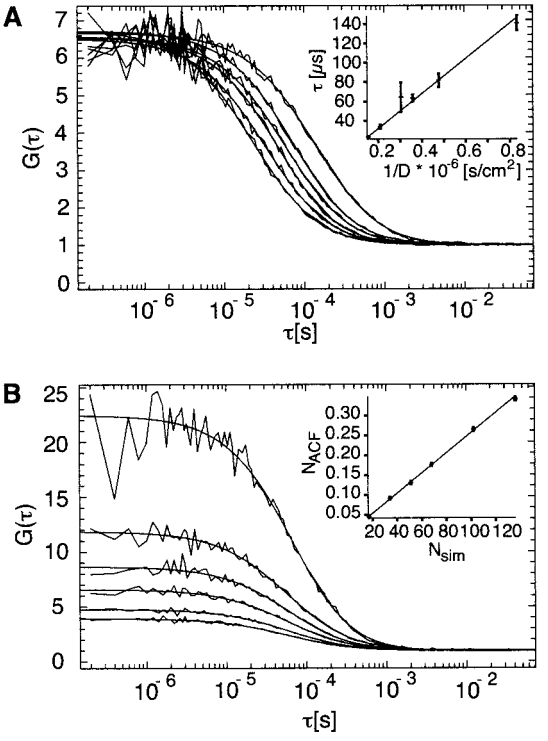

FIGURE 4 (*A*) One-component simulations for different diffusion coefficients (D = 1.2, 2.1, 2.7, 3.3, 4.8, 6.5 × 10^{-10} m^2/s). Simulation time 6.7 s, counts per particle per second is 35 kHz. The diffusion time increases with decreasing diffusion coefficient. In the inset, the diffusion time is depicted versus 1/D (Eq. 3). (*B*) One-component simulations for different concentrations (0.26, 0.51, 0.76, 1.01, 1.51, 2.01 nM) corresponding to different numbers of simulated particles N_{sim} in the simulated spherical volume of 3-μm radius (N_{sim}: 18, 35, 52, 69, 103, 137). $G(\tau)$ is the ACF, τ is the delay time. N_{ACF} is the number of particles in the observation volume obtained by fitting the ACF. The simulation time is 6.7 s, the counts per particle per second are 35 kHz. In the inset, the number of observed particles is depicted versus the number of simulated particles. The number of particles obtained by the ACF increases linearly with the concentration.

RESULTS AND DISCUSSION

Simulations

To confirm that the computer simulations correctly reproduce the features of real FCS measurements, several test simulations were performed for one-component systems varying the diffusion coefficient, number of particles in the sample volume, absorption cross section of the chromophore, and total measurement time. The results of the different simulations show that the correlation time τ_D is inversely proportional to the diffusion coefficient D, as predicted by Eq. 3 (Fig. 4 *A*). Equally, the number of particles fitted by Eq. 2 depends linearly on the number of particles in the observation volume, as one would expect (Fig. 4 *B*). The count rates depend linearly on the cross section of the particles, and the noise in the measurement decreases with the square root of the measurement time (data not shown).

The proportionality factor γ was calculated for a GGG and for a GLB profile. For the GGG profile, the integration can be performed with or without a pinhole (CEF(r, z) = 1 in Eq. 21). A value of $\gamma = 0.3535$ was obtained without a pinhole (theoretical value $1/\sqrt{8} \approx 0.3536$) and $\gamma = 0.3533$ with pinhole. The agreement with theory is excellent, demonstrating that the pinhole actually has little effect on the GGG profile. For the GLB profile, the case is different; here an integration cannot be performed because Eq. 5 diverges. This is due to the exponential in Eq. 9, which depends not only on the radial coordinate r but also on the axial coordinate z over the beam waist $w(z)$. If the exponential depended solely on the radial coordinate r, and $w(z)$ was replaced by w_0, the integral could be solved analytically yielding $\gamma = 0.25$ (Kask et al., 1997). Nevertheless, when a pinhole of 50 μm is assumed, a numerical integration is possible because points far away from the focus are suppressed by the characteristic CEF of the pinhole yielding $\gamma = 0.2760$. The values of the integration did not change when the grid spacing, on which the intensity and CEF values are calculated, were reduced from 5 to 2.5 nm in z and r directions. When the simulation volume was changed to a 2- or a 6-μm radius, the value of γ changed by less than 2% to $\gamma = 0.2815$ and $\gamma = 0.2707$, respectively. This supports the assumption that a 3-μm radius sphere is sufficiently large to include the whole laser profile and does only

minimally influence γ. A larger influence on γ is the pinhole size (Table 2). With $\gamma = 0.2760$, the apparent average number of particles in the confocal volume that are expected from the simulations can be calculated to $N = 0.144$.

The geometry factor K can be calculated from Eq. 9 and the CEF. The distance on the optical axis where the intensity has dropped by $1/e^2$ can be calculated to $z_0 = 1.056$ μm. Taking the CEF into account, the distance on the optical axis where the detected intensity has dropped by $1/e^2$ decreases and can be calculated to $z_0 = 0.511$ μm, leading to a theoretical value for the geometry factor of $K \approx 2.0$ ($w_0 = 261.5$ nm).

For the simulations, we found, on average, the values $N = 0.187 \pm 0.002$ and $K = 2.7 \pm 0.6$ (10 one-component simulations). The discrepancy between the calculation and simulations of the number of particles in the observation volume N is closely related to the difference in the factor K. Eq. 2 that was used to fit the simulated data is a model that assumes a GGG profile. This is only an approximation, and, as was shown above, the factor γ depends strongly on the actual profile used. The factor γ is difficult to determine for an experimental setup, but the geometry factor K is more easily accessible. Therefore, Rigler et al. (1993) proposed to approximate the focal volume by a cylinder with length $2z_0$ and radius w_0. The volume $V = 2\pi K w_0^3$ relates, then, directly to the apparent number of particles measured, and an independent measurement of the factor γ is unnecessary. For $K = 2.7$, a volume of $V = 0.30$ fl and an average number of 0.18 molecules per nM is obtained. For $K = 2.0$, $V = 0.22$ fl and an average number of 0.14 molecules per nM is calculated. Although the non-Gaussian intensity profile leads to deviations, the results are in excellent agreement with the values given above and confirm the more practical approximation of Rigler et al. (1993).

TABLE 2 Simulations for varying pinhole radii

r_{ph} [μm]	τ_D [μs]	χ_v^2	K	χ_v^2 ($K = 2.7$)	γ
5	14.4	3.99	4542.5	4.65	0.0232
10	44.3	1.13	3.2	1.12	0.0897
15	46.7	0.89	2.2	0.92	0.1791
20	52.9 (40.6)	0.89 (0.49)	2.1 (4.0)	0.96	0.2478
25	58.8 (61.2)	0.84 (0.54)	2.7 (4.0)	0.84	0.2760
30	70.0	0.76	2.4	0.78	0.2801
35	84.1	0.89	2.2	0.93	0.2754
40	83.0 (89.2)	0.84 (0.87)	3.3 (5.5)	0.90	0.2681
45	89.9	1.10	2.8	1.10	0.2599
50	96.9	1.04	2.5	1.05	0.2515
60	101.7	1.87	3.1	1.87	0.2351
70	120.8	2.63	3.3	2.63	0.2200
80	116.0	3.00	4.9	3.13	0.2065
150	150.3	8.7	9.0	8.91	0.1472
250	156.0	18.6	766.3	18.82	0.1137

r_{ph} is the pinhole radius, τ_D is the diffusion time, χ_v^2 is the fitted value when the geometry factor K is a free parameter. γ is the calculated correction factor for the ACF due to the intensity distribution in the focal volume. The values for K are given in the corresponding column K, and χ_v^2 ($K = 2.7$) is the value for χ_v^2 when the geometry factor K is fixed to 2.7. For $r_{ph} = 15$, 25, and 45 μm, experimental values were published elsewhere (Rigler et al., 1993) and are given for comparison in parentheses. A clear increase of χ_v^2 values can be seen for $r_{ph} < 15$ μm and $r_{ph} > 40$ μm. This increase shows that the model used (Eq. 2), which is based on a Gaussian intensity distribution in three dimension, is no longer valid.

To further investigate the influence of the pinhole size on the adequacy of Eq. 2 as an approximation, we performed simulations for different pinhole radii r_{ph} ranging between 5 and 250 μm (Table 2). The simulations show that χ_v^2 increases for $r_{ph} < 15$ μm or $r_{ph} > 40$ μm but shows only small variations in between. Therefore, the approximation of the GLB profile by a GGG profile, as assumed in Eq. 2, is only valid between 15 and 40 μm. For r_{ph} values outside of this range, χ_v^2 increases strongly. This is not only true for χ_v^2 but also for the fitted geometry factor K, which significantly deviates from the expected value of 2.7 ± 0.6 for $r_{ph} < 15$ μm and $r_{ph} \geq 70$ μm. The deviation for small pinhole radii is expected because the projection into sample space of a pinhole with a radius of 16.5 μm is just the size of the laser beam ($w_0 = 261.5$ nm, magnification 63). For smaller radii, part of the laser profile is cut off by the pinhole and the model is not correct anymore. For larger pinhole radii, the Lorentzian distribution of the laser beam along the optical axis is no longer influenced by the pinhole, and the difference between the approximation of the focus with a Gaussian profile along the optical axis becomes noticeable. Experimentally, this effect was confirmed for a pinhole radius of 45 μm (Rigler et al., 1993).

The two-component simulations are summarized in Table 1. Each of the components was first tested in a one-component simulation to determine its diffusion time τ_D and the accuracy of the simulation. The simulations were fitted by weighting with σ_{IT} (see discussion below), which gives the smallest error for τ_D; the values were averaged over 10 simulations. These expected values are a good reference for the other tests. It was necessary to fix the factor K to a reasonable value for all but simple one-component simulations. In the latter case, the factor K can be determined with good accuracy. For more complex systems, the fits are not sensitive to this factor and, usually, K tends to diverge and influences the other parameters, thus biasing the correlation times (and triplet lifetimes if present). The number of particles N are less influenced by K, as can be seen from Eq. 2.

Measurements

FCS measurements of an aqueous solution of Rho 6G showed a correlation time of 56.6 ± 1.4 μs, a geometry factor $K = 5.8 \pm 0.8$, $N = 0.399 \pm 0.046$ particles per observation volume, and a $\chi_v^2 = 0.65 \pm 0.12$ (σ_{IT}). The characteristics of the different SDs are discussed in the next section in the context of the simulations. Results are shown in Table 3.

TABLE 3 Comparison of the different procedures to calculate the standard deviation for simulations and measurements

	N	τ_D	K	G_∞	χ^2_v
Experiments					
σ_{AV}	0.398 ± 0.046	56.5 ± 1.4	5.7 ± 0.6	1.004 ± 0.001	0.96 ± 0.15
σ_{IT}	0.399 ± 0.046	56.6 ± 1.4	5.8 ± 0.8	1.003 ± 0.002	0.65 ± 0.12
σ_{Koppel}	0.398 ± 0.046	56.5 ± 1.4	6.1 ± 0.9	1.002 ± 0.002	0.49 ± 0.10
σ^*_{AV}	0.395 ± 0.045	55.8 ± 1.6	31.5 ± 41.2	0.993 ± 0.011	1.21 ± 0.54
Simulations					
σ_{AV}	0.187 ± 0.002	58.7 ± 4.4	2.7 ± 0.6	0.993 ± 0.003	1.07 ± 0.14
σ_{IT}	0.187 ± 0.002	58.8 ± 3.9	2.7 ± 0.6	0.992 ± 0.004	0.84 ± 0.12
σ_{Koppel}	0.187 ± 0.002	58.1 ± 3.9	2.8 ± 0.7	0.991 ± 0.006	0.75 ± 0.13

ACFs were calculated for 10 simulations and 10 measurements. The fits to the ACFs were weighted with one of several alternatives, as described in the text. σ_{AV} is the SD calculated by statistically evaluating 10 different ACFs, σ_{IT} was calculated directly from the intensity traces (Eq. 18), and σ_{Koppel} is the estimate of the SD due to Koppel's formula (Eq. 17). For the measurement, σ^*_{AV} was calculated additionally (Eqs. 19–21).
Parameters for the simulations: $D = 2.7 \times 10^{-10}$ m^2/s, $P = 100$ μW, $\lambda = 514.5$ nm, $\sigma_{abs} = 2.2 \times 10^{-20}$ m^2, $q_f = 0.98$, simulation time is 6.7 s, 69 particles are simulated in a sphere of 3-μm radius (corresponding to a concentration of 1 nM), a pinhole with 50-μm diameter was assumed, the shortest channel time was 0.2 μs, 128 channels were used.
Experimental conditions: Aqueous solution of Rho 6G ($D = 2.8 \times 10^{-10}$ m^2/s, $\sigma_{abs} = 2.2 \times 10^{-20}$ m^2, $q_f = 0.98$), $P = 100$ μW, $\lambda = 514.5$ nm, the measurement time was 10 s, the channel width was 5 μs, a pinhole with 50-μm diameter was installed, 78 channels were used. The first channel (correlation time 0) was left out because of shot noise contributions.

The standard deviations

In this work, we calculated the SD of ACFs in different ways and compared the corresponding results to the well-known approximation of Koppel (1974), denoted as σ_{Koppel} (Tables 1 and 3). In a first approach, the SD was obtained directly from intensity data (σ_{IT}) by determining the standard error of the mean of each point in the ACF (Eq. 18). In FCS experiments, this computation is usually not possible, because the commercially available hardware correlators neither calculate the SD nor do they give access to the intensity data. Furthermore, it is not practical to store all the intensity data for later use because of the memory needed. Three hundred million integer values obtained during a typical experiment with 60-s total measurement time at 0.2-μs sampling rate cannot be stored efficiently, especially when usually 10 measurements are taken for every experiment. Another possibility is to register only the arrival times of photons (Eid et al., 2000) thus decreasing the number of data points to about 10^3–10^5 values per second, but still leaving the very high number of about 6×10^4–6×10^6 data points per 60-s measurement time. Using σ_{IT} (Eq. 14) the SD can be calculated directly from the intensity data during the correlation with only little changes in the correlator structure. If one stores the sum of the correlation values and their square value for every channel, the SD can easily be calculated after the experiment, resulting in only 256 additional values that have to be stored (when 128 channels are used). Thus, the SD can be calculated online together with the ACF.

In the second method, the SD is calculated by averaging over several measured ACFs. This approach delivers σ_{AV}, a measured SD that can serve as a standard for comparison with the other methods. However, this advantage is partly lost because several ACFs have to be measured, increasing the measurement time considerably. Because this is not acceptable, especially when large numbers of samples have to be investigated, we use this SD only as a comparative standard.

In the following, we present a third method to calculate the SD; it requires only a single FCS experiment, i.e., minimal measuring time. During one measurement, this approach calculates not only the ACF for the whole measurement, but also ACFs for a number L of subsets of the measurement of equal length. By averaging over these subsets, their SD can be calculated and is denoted by σ^*_{AV}. Because the whole measurement is L times longer than that of individual subsets and the SD decreases with the square root of the measurement time, it is now possible to calculate σ^*_{AV}, the SD for the ACF of the whole measurement, by dividing the SD of the subsets by $\sqrt{L}$ (Eq. 22). It should be noted that there is a fundamental difference between σ_{AV} and σ^*_{AV}. Although both SDs are eventually calculated for an ACF of measurement time T, σ_{AV} is calculated by averaging several (n_{exp}) ACFs of measurement time T, resulting in a total measurement time of $n_{exp}T$, and σ^*_{AV} is calculated for an ACF of measurement time T/L, and is then scaled by the factor $\sqrt{L}$. Thus, the total measurement time for the estimation of σ^*_{AV} is only T. Because σ^*_{AV} is determined from fewer data points than σ_{AV}, the error in the estimation of σ^*_{AV} is larger than for σ_{AV}, although σ^*_{AV} has, on average, the same mean value as σ_{AV}. This can lead to differences when the two SDs are used in the fitting procedure (Table 3).

The different SDs for one-component simulations are shown in Fig. 5 *A*. σ_{Koppel} decreases with increasing delay time for the range between 0 and 1 ms and then increases again for delay times longer than 1 ms. The SDs σ_{IT}, σ_{AV}, and σ^*_{AV} show the same behavior as σ_{Koppel} between 0- and 1-ms delay times, but remain constant for delay times longer than 1 ms (σ^*_{AV}, not shown in Fig. 5 *A*, has the same characteristics as σ_{AV} albeit with higher deviations). The increase in the SD for long delay times as predicted by

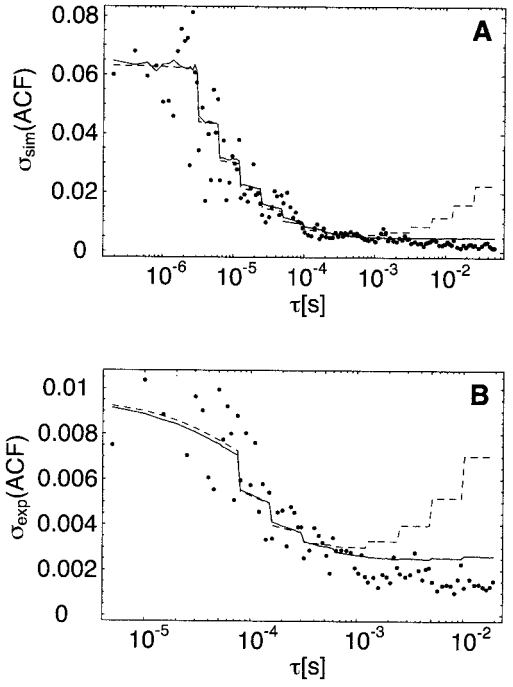

FIGURE 5 The different methods to calculate the SD in FCS. σ_{Koppel} (*dashed line*), σ_{IT} (*solid line*), and σ_{AV} (*points*) of (*A*) simulated and (*B*) experimental autocorrelation functions calculated according to the procedures described in the text and plotted versus the delay time. In the simulated as well as in the experimental case, σ_{Koppel} deviates strongly from the expected value σ_{AV}, which is calculated by averaging 10 individual ACFs. σ_{IT} is much closer to σ_{AV} but deviates as well for long delay times. Parameters for simulations in (*A*) and experimental conditions in (*B*) are as given in Table 3.

σ_{Koppel} should result in an increase in the noise for these delay channels. But, to our knowledge and experience, this increase has not been observed experimentally. For FCS measurements in solution, the ACF is smooth at long delay times and does not show the fluctuations predicted by σ_{Koppel} (Meseth et al., 1999). Actually, σ_{Koppel} is a good approximation for the short time range but fails to predict the long time behavior.

A good parameter to judge the reliability of the different SDs is the value of χ^2_v (Table 3). χ^2_v should tend toward 1 for a good fit when the SD is correctly estimated. It is not surprising that this is actually the case for σ_{AV} and σ^*_{AV}; σ_{AV} is calculated as an average of several measurements and is thus in accord with the definition of a SD; σ^*_{AV} is an estimation of σ_{AV} by averaging over ACFs of shorter measurement time. It reproduces the average characteristics of σ_{AV} but with higher uncertainties, as reflected in the higher spread of χ^2_v values. For σ_{Koppel}, the χ^2_v values are typically well below 1 because of the overestimation of the SD for long delay times. For σ_{IT}, the values of χ^2_v are larger than for σ_{Koppel} but still below 1. The standard error of the mean is only then a correct estimation of the SD if the samples are uncorrelated (Davenport and Root, 1958). This is certainly not the case for our measurements and leads to the observed deviations. However, it is not clear why these deviations are larger at long than at short delay times, where σ_{IT} agrees very well with σ_{AV}. This should be the subject of further studies because σ_{IT} represents a convenient method to calculate the SD online and needs much less computation power than in the case of σ^*_{AV}, which has to be determined by averaging several ACFs online.

The measurements show the same characteristics as the simulations (Fig. 5 *B*) and support these arguments. The difference in the shape of the SDs for the simulations and the experiments are solely due to the different minimal channel width. This is reflected by σ_{Koppel}, which is a theoretical function that does not depend on the actual measurement but only on average values (average count rate, diffusion time, number of particles, and channel width of the correlator). Because all parameters, with the exception of the channel width (0.2 μs for the simulations, 5 μs for the experiments), were virtually unchanged for simulations and experiments, the difference in the SDs is caused by the change of the time base and not by an artifact of the simulations.

The influence of the background signal on the SD was determined by repeating the same one-component simulation five times while adding background signals of 0.2, 0.4, 0.6, 0.8, and 1.0 kHz, a range typically found in FCS measurements. With increasing background signal, the amplitude of the ACF decreases, suggesting an apparent increase in the number of particles (Koppel, 1974). It can be observed that, with a higher background signal present, the difference between σ_{IT} and σ_{Koppel} increases as well for short delay times (0.2–10 μs, data not shown). This discrepancy is a direct consequence of the fact that σ_{Koppel} considers the background signal only in form of the average number $\langle n \rangle$ of counts per channel, which slightly decreases the value of σ_{Koppel} (Koppel's formula is derived for the case that the background is negligible). The other SDs, on the contrary, are calculated from the intensity traces or the ACFs and are directly influenced by the additional error introduced by the background signal.

Influence of the different standard deviations on the fit results

As discussed in the previous section, the different fits for the one-component simulations differ mainly in their χ^2_v values (Table 3). The same fit values were obtained ($N = 0.187 \pm 0.002$; $\tau_D = 58.5 \pm 4.4$ μs; $K = 2.7 \pm 0.7$; $G_\infty = 0.992 \pm 0.006$) independent of which of the different SDs were used. Even when no data weighting is applied (χ^2_v is not defined for this case) only the value of τ_D changes significantly (69.7 ± 14.1 μs).

For the real FCS experiments, which were also evaluated by one-component models, the results are similar. Only χ^2_v differs markedly for the individual cases, whereas the fit parameters are the same within the margin of error ($N =$

0.398 ± 0.046, $\tau_D = 56.4 \pm 1.4$ μs, $G_\infty = 1.001 \pm 0.004$). The case is different for the two-component systems (Table 1). For the first investigated system A, in which the diffusion coefficients of the two components differ by almost two orders of magnitude, the different methods of data weighting during the fit do not influence the results considerably. All fits using weighted data recover the parameters for the diffusion times τ_{D1} and τ_{D2} quite well with uncertainties of about 11% for the faster component and 20% for the slower component. The parameters and the errors do not change even for nonweighted fits. For system B, in which the diffusion coefficients of the two components differ by only a factor of 4, two effects can be observed. First, the error for the fast component increases to ~20% and, for the slow component, to 31%. These larger errors are due to the smaller separation between the diffusion coefficients, which are now close to the resolution limit of FCS. Second, the average values of the fit parameters converge slowly, depending on the weighting method, toward the expected value as determined by calculations and one-component simulations while the errors decrease in absolute value (but only marginally in relative value). The best values are obtained by σ_{AV}, the worst values by fits without data weighting. If the diffusion time of the fast component is fixed to its expected value, the data weighting has no influence, and the relative errors in the parameter recovery are the same for all methods, 13–16% in system A and 11–12% in system B.

These examples demonstrate that, as long as the system is sufficiently simple (only one component present, or several components are present and the diffusion times differ significantly) all SDs described in this work, including σ_{Koppel}, are equally good for data weighting and deliver the same parameter estimations within the margins of error. The situation is, however, different for more complex systems, e.g., those composed of several components with diffusion times that are close to the limit to be distinguishable by FCS.

Under these conditions, the uncertainty of the estimated parameters increases compared to systems that contain particles with clearly different diffusion constants. Furthermore, the fitted parameters converge to their expected value depending on the data-weighting procedure. The parameters are worst for fits without data weighting and best for weighting with σ_{AV}.

All presented methods to calculate the SD in FCS experiments have advantages and disadvantages. The correct SD for ACFs is σ_{AV} and should be used if possible, but it increases the measuring time for a FCS experiment several fold. The conventional approach to use σ_{Koppel} fails to predict the SD correctly for long delay times; it delivers larger error margins for the fitted parameters than the other methods when complex systems close to the resolution limit of FCS are investigated. If σ_{IT} and σ^*_{AV} should be calculated, the presently available correlators need to be modified. This is straightforward if the correlators are software-based but it might be difficult for hardware correlators. σ_{IT} still overestimates the SD for long delay times but to a much lesser extent than σ_{Koppel}. σ^*_{AV} yields similar results as σ_{AV} but is only an estimate for σ_{AV} and comprises larger error margins for fitted parameters. A further advantage of σ_{AV} and σ^*_{AV} is that they result in χ^2_v values that converge to 1 when the fit is correct. Although the χ^2_v test is only one of many possibilities to test the goodness of a fit, it is nonetheless widely used. It needs a correct estimation of the SD, otherwise the convergence value of χ^2_v is not known, and other tests must be used in parallel.

CONCLUSIONS

The major objective of this work was to show that the correct SD of fluorescence correlation measurements is crucial for accurate data evaluation, and that the currently used model, derived by Koppel (1974), is an approximation that does not fulfill these requirements in many cases. We therefore presented a simulation program that takes account of the most important features of FCS. This program was used for the study of the SD of autocorrelation functions obtained both by simulations and measurements. Several different methods to calculate the SD were presented and compared with the established approximation of Koppel (σ_{Koppel}). These methods included the calculation of the SD directly from intensity traces (σ_{IT}), by the statistical evaluation of several ACFs (σ_{AV}), and by the division of one measurement in several subsets and the subsequent error estimation from these subsets (σ^*_{AV}).

It was shown that data weighting is necessary and improves parameter evaluation in FCS. The presently used formula—σ_{Koppel}—is an approximation but does not correctly describe the SD for long delay times. The methods presented in this work describe the SD correctly in all time ranges and yield the same characteristics but differ in some respects. Although σ_{AV} represents the real SD, it needs several ACFs for its calculation and is thus more time consuming. Although σ^*_{AV} shows higher errors, it is a good estimation of the SD and can be calculated from one ACF, eliminating the need of several measurements. σ_{IT} can be calculated for one ACF and shows similar results as σ_{AV} but overestimates the SD slightly for long delay times.

However, independent of the evaluation scheme, the average values of the parameters are recovered quite well within the margins of error but the average value of the parameters converges slowly to the expected value from nonweighted fits, which yields the worst, to σ_{AV}, which yields the best estimates. This convergence can be important, and we expect to find other more complex systems, e.g., biological systems, where more than one component is present, or diffusion times show only small differences, where this increase in accuracy can be crucial in the decision between two hypotheses. Therefore, data weighting is important for fitting models to experimental ACFs. Furthermore, the χ^2_v values are close to 1 only for σ_{AV}

and σ^*_{AV}. This shows not only that these SDs determine the actual SD correctly but it is important for deciding if a model is adequate.

Which method finally should be used depends on the particular situation. When measuring time is not a limiting factor, σ_{AV} is the best choice because it calculates the correct SD. In addition, σ_{AV} can be used with existing hardware correlators. If data-acquisition time should be minimized, σ^*_{AV} and σ_{IT} are the SDs of choice, but it has to be borne in mind that present hardware correlators do not allow this calculation. Therefore, either software correlators have to be used for online measurements, or recorded intensity traces have to be treated offline. Both, σ^*_{AV} and σ_{IT}, improve the parameter estimation over σ_{Koppel} and need only one ACF for their calculation. If none of the above-mentioned procedures can be applied, σ_{Koppel} is the proper choice, which still improves the parameter estimation over nonweighted fits, although χ^2_v values will be underestimated ($\chi^2_v < 1$).

In the future, a further step should be taken to improve the data evaluation in FCS. The fitting models used in FCS are still only approximations of the actual ACFs and all assume a beam profile that shows Gaussian characteristics in all three Cartesian coordinate axes. But this is not the case for a laser beam profile, especially if aberrations are present in the optical system. If one could actually use the measured point spread function of a setup to numerically calculate the expected model for an ACF, the errors inherent in the presently used models could be avoided. With the computer power and speed increasing, this could well be the next step in improving data-evaluation schemes for FCS.

The work was financially supported by the Swiss National Science Foundation 31-57023.99.

REFERENCES

Aragon, S. R., and R. Pecora. 1976. Fluorescence correlation spectroscopy as a probe of molecular dynamics. *J. Chem. Phys.* 64:1791–1803.

Auer, M., K. J. Moore, F. J. Meyer-Almes, R. Guenther, A. J. Pope, and K. A. Stoeckli. 1998. Fluorescence correlation spectroscopy: lead discovery by miniaturized HTS. *Drug Disc. Today*. 3:457–465.

Bevington, P. R., and D. K. Robinson. 1992. Data Reduction and Error Analysis for the Physical Sciences. McGraw Hill, New York. 194–197.

Bronstein, I. N., and K. A. Semendjajew. 1989. Taschenbuch der Mathematik. BSB Teubner, Leipzig, Germany. 280–281.

Chen, Y., J. D. Muller, P. T. C. So, and E. Gratton. 1999. The photon counting histogram in fluorescence fluctuation spectroscopy. *Biophys. J.* 77:553–567.

Davenport, W. B. J., and W. L. Root. 1958. An Introduction to the Theory of Random Signals and Noise. McGraw-Hill, New York. 76–86.

Di Cera, E. 1992. Use of weighting functions in data fitting. *In* Numerical Computer Methods. L. Brand and M. L. Johnson, editors. Academic Press, Inc., London, UK. 68–87.

Eggeling, C., J. Widengren, R. Rigler, and C. A. M. Seidel. 1998. Photobleaching of fluorescent dyes under conditions used for single-molecule detection—evidence of 2-step photolysis. *Anal. Chem.* 70:2651–2659.

Eid, J. S., J. D. Müller, and E. Gratton. 2000. Data acquisition card for fluctuation correlation spectroscopy allowing full access to the detected photon sequence. *Rev. Sci. Instr.* 71:361–368.

Grossmann, S. 1988. Mathematischer Einführungskurs für die Physik. BG Teubner, Stuttgart, Germany.

Hansen, R. L., X. R. Zhu, and J. M. Harris. 1998. Fluorescence correlation spectroscopy with patterned photoexcitation for measuring solution diffusion coefficients of robust fluorophores. *Anal. Chem.* 70:1281–1287.

Kask, P., R. Gunther, and P. Axhausen. 1997. Statistical accuracy in fluorescence fluctuation experiments. *Eur. Biophys. J.* 25:163–169.

Klingler, J., and T. Friedrich. 1997. Site-specific interaction of thrombin and inhibitors observed by fluorescence correlation spectroscopy. *Biophys. J.* 73:2195–2200.

Koppel, D. E. 1974. Statistical accuracy in fluorescence correlation spectroscopy. *Phys. Rev. A.* 10:1938–1945.

Magde, D., E. L. Elson, and W. W. Webb. 1972. Thermodynamic fluctuations in a reacting system: measurements by fluorescence correlation spectroscopy. *Phys. Rev. Lett.* 29:705–708.

Mandel, L., and E. Wolf. 1995. Optical Coherence and Quantum Optics. Cambridge University Press, Cambridge. 449–452.

Meseth, U., T. Wohland, R. Rigler, and H. Vogel. 1999. Resolution of fluorescence correlation measurements. *Biophys. J.* 76:1619–1631.

Press, W. H., S. A. Teukolsky, W. T. Vetterling, and B. P. Flannery. 1992. Numerical Recipes in C: The Art of Scientific Computing. Cambridge University Press, Cambridge, U.K. 275–296.

Qian, H. 1990. On the statistics of fluorescence correlation spectroscopy. *Biophys. Chem.* 38:49–57.

Qian, H., and E. Elson. 1991. Analysis of confocal laser-microscope optics for 3-D fluorescence correlation spectroscopy. *Appl. Opt.* 30: 1185–1195.

Rauer, B., E. Neumann, J. Widengren, and R. Rigler. 1996. Fluorescence correlation spectrometry of the interaction kinetics of tetramethylrhodamin α-bungarotoxin with *Torpedo califonica* acetylchoine receptor. *Biophys. Chem.* 58:3–12.

Rigler, R., U. Mets, J. Widengren, and P. Kask. 1993. Fluorescence correlation spectroscopy with high count rate and low-background—analysis of translational diffusion. *Eur. Biophys. J.* 22:169–175.

Rogers, M. V. 1997. Light on high throughput screening: fluorescence-based assay technologies. *Drug Disc. Today.* 2:156–160.

Saleh, B. E. A., and M. C. Teich. 1991. Fundamentals of Photonics. John Wiley & Sons, Inc., New York. 81–92.

Schätzel, K. 1985. New concepts in correlator design. *Inst. Phys. Conf. Ser.* 77:175–184.

Schätzel, K. 1991. Noise on multiple-tau photon correlation data. *In* Photon Correlation Spectroscopy Multicomponent System. K. S. Schmitz, editor. *SPIE.* 1430:109–115.

Schätzel, K., M. Drewel, and S. Stimac. 1988. Photon correlation measurements at large lag times: improving statistical accuracy. *J. Mod. Opt.* 35:711–718.

Siegman, A. E. 1986. Lasers. California University Books, Sausalito, CA. 663–680.

Sterrer, S., and K. Henco. 1997. Minireview: fluorescence correlation spectroscopy (FCS)—a highly sensitive method to analyze drug/target interactions. *J. Recept. Signal Transduct. Res.* 17:511–520.

Thompson, N. L. 1991. Fluorescence correlation spectroscopy. *In* Topics in Fluorescence Spectroscopy, Vol. 1. Techniques. J. R. Lakowicz, editor. Plenum Press, New York. 337–378.

Van Craenenbroeck, E., and Y. Engelborghs. 1999. Quantitative characterization of the binding of fluorescently labeled colchicine to tubulin in vitro using fluorescence correlation spectroscopy. *Biochemistry.* 38: 5082–5088.

Winkler, T., U. Kettling, A. Koltermann, and M. Eigen. 1999. Confocal fluorescence coincidence analysis—an approach to ultra high-throughput screening. *Proc. Natl. Acad. Sci. U.S.A.* 96:1375–1378.

Wohland, T., K. Friedrich, R. Hovius, and H. Vogel. 1999. Study of ligand receptor interactions by fluorescence correlation spectroscopy with different fluorophores: evidence that the homopentameric 5-hydroxytryptamine type 3As receptor binds only one ligand. *Biochemistry.* 38: 8671–8681.